

Traffic jams induced by rare switching events in two-lane transport

Tobias Reichenbach, Erwin Frey, and Thomas Franosch

*Arnold Sommerfeld Center for Theoretical Physics (ASC) and Center for NanoScience (CeNS),
Department of Physics, Ludwig-Maximilians-Universität München,
Theresienstrasse 37, D-80333 München, Germany*

(Dated: May 26, 2019)

We investigate a model for driven exclusion processes where internal states are assigned to the particles. The latter account for diverse situations, ranging from spin states in spintronics to parallel lanes in intracellular or vehicular traffic. Introducing a coupling between the internal states by allowing particles to switch from one to another induces an intriguing polarization phenomenon. In a mesoscopic scaling, a rich stationary regime for the density profiles is discovered, with localized domain walls in the density profile of one of the internal states being feasible. We derive the shape of the density profiles as well as resulting phase diagrams analytically by a mean-field approximation and a continuum limit. Continuous as well as discontinuous lines of phase transition emerge, their intersections induce multicritical behavior.

PACS numbers: 05.40.-a, 05.60.-k 64.60.-i, 72.25.-b

I. INTRODUCTION

Non-equilibrium critical phenomena arise in a broad variety of systems, including non-equilibrium growth models [1], percolation-like processes [2], kinetic Ising models [3], diffusion limited chemical reactions [4], and driven diffusive systems [5]. The latter provide models for transport processes ranging from biological systems, like the motion of ribosomes along a *m*-RNA chain [6] or processive motors walking along cytoskeletal filaments [7, 8], to vehicular traffic [9, 10]. In this work, we focus on the steady-state properties of such one-dimensional transport models, for which the Totally Asymmetric Simple Exclusion Process (TASEP) has emerged as a paradigm (for reviews see e.g. [11, 12, 13]). There, particles move unidirectionally from left to right on a one-dimensional lattice, interacting through on-site exclusion. The entrance/exit rates at the open left/right boundary control the system's behavior; tuning them, one encounters different non-equilibrium phases for the particle densities [14].

Intense theoretical research has been devoted to the classification of such non-equilibrium phenomena. For example, within the context of reaction-diffusion systems, there is strong evidence that phase transitions from an active to an absorbing state can be characterized in terms of only a few universality classes, the most important being the one of directed percolation (DP) [15]. To search for novel critical behavior, fruitful results have been obtained by coupling two reaction-diffusion systems [16, 17], each undergoing the active to absorbing phase transition. Due to the coupling, the system exhibits a multicritical point with unusual critical behavior.

We want to stress that already in equilibrium physics seminal insights have been gained by coupling identical systems. For instance, spin-ladders incorporate several Heisenberg spin chains [18]. There, quantum effects lead to a sensitive dependence on the chain number: for even ones a finite energy gap between the ground state and

the lowest excitation emerges whereas gapless excitations dominate the low-temperature behavior if the number of spin chains is odd.

In this work, we generalize the Totally Asymmetric Exclusion Process (TASEP) in a way that particles possess two internal states; a short account of this work was recently published in our PRL [19]. Allowing particles to occasionally switch from one internal state to the other induces a coupling between the latter; indeed, the model may alternatively be regarded as two coupled TASEPs. When independent, each of them separately undergoes boundary-induced phase transitions [14]. The coupling is expected to induce novel phenomena, which are the subject of the present work.

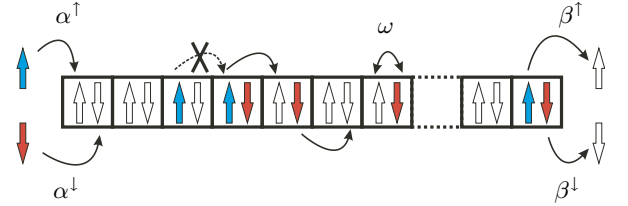


FIG. 1: (Color online) Illustration of an exclusion model with two internal states, adopting the language of spin transport. Particles in states \uparrow (\downarrow) enter with rates α^\uparrow (α^\downarrow), move unidirectionally to the right within the lattice, may flip at rate ω and leave the system at rates β^\uparrow (β^\downarrow), always respecting Pauli's exclusion principle.

Exclusion is introduced by allowing multiple occupancy of lattice sites only if particles are in different internal states. Viewing the latter as spin-1/2 states, i.e. spin-up (\uparrow) and spin-down (\downarrow), this directly translates into Pauli's exclusion principle; see Fig. 1. Indeed, the exclusion process presented in this work may serve as a model for semiclassical transport in mesoscopic quantum systems [20], like hopping transport in chains of quantum dots in the presence of an applied field [21]. Our model incorporates the quantum nature of the particles

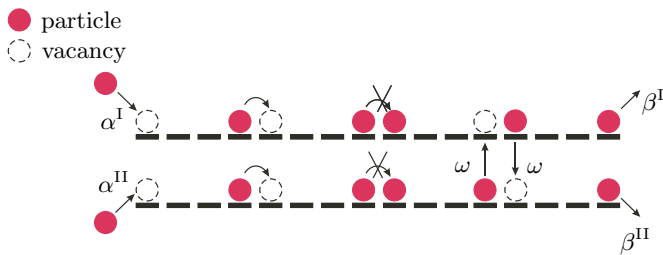


FIG. 2: Illustration of the two-lane interpretation. We label the upper lane as lane I and the lower one as lane II. They possess individual entering rates, α^I resp. α^{II} as well as exiting rates, β^I resp. β^{II} .

through Pauli's exclusion principle, though phase coherence is ignored. A surprising analogy to a simple spintronics scheme, the Datta-Das spin field-effect transistor [20], holds. There, electrons move unidirectionally through a ferromagnetic metal or a semiconductor. The polarization of the electrons is controllable by a source for spin injection, a drain for spin extraction as well as a gate in the form of a tunable magnetic field that controls the strength of spin precession. In our model, this is mimicked by considering the spin-flip rate as a control parameter.

The model is potentially relevant within biological contexts, as well. In intracellular traffic [7, 22], molecular motors walking on parallel filaments may detach from one lane and attach on another, resulting in an effective switching between the lanes. In our model, identifying the two internal states with different lanes, one recovers a transport model on two lanes with simple site exclusion. In the same way, the system presented in this work serves as a highly simplified cartoon model of multi-lane highway traffic taking lane switching into account [9, 10].

Significant insight into multi-lane traffic has been achieved (see [9, 10] and references therein). In particular, novel phases have been discovered in the case of indirect coupling, i.e. the velocity of the particles depends on the configuration on the neighboring lane [23, 24, 25]. Recently, models have been presented that allow particles to switch between lanes, and the transport properties have in part been rationalized in terms of an effective single lane TASEP [26, 27, 28]. There, the case of strong coupling has been investigated: the timescale of lane switching events is the same as of forward hopping. In our model, we explicitly want to ensure a competition between the boundary processes and the switching between the internal states. We therefore employ a mesoscopic scaling, i.e. we consider the case where the switching events are rare as compared to forward hopping. As a result of the scaling, an intriguing polarization phenomenon emerges [19], which is discussed in detail in this article.

The outline of the present paper is the following. In Sec. II we introduce the model in the context of spin transport as well as two-lane traffic. Symmetries and currents are discussed, which play a key role in the fol-

lowing analysis. Section III describes in detail the mean-field approximation and the differential equations for the densities obtained therefrom through a continuum limit. The mesoscopic scaling is motivated and introduced, the details of the analytic solution for the spatial density profiles being condensed in Appendix A. We obtain the generic form of the density profiles in Sec. IV, and compare our analytic results to stochastic simulations. The polarization phenomenon is encountered and its origin is rationalized in terms of singularities in coupled differential equations. We partition the full parameter space into three distinct regions, and observe a delocalization transition. The methods to calculate the phase boundaries analytically are developed simultaneously. Section V presents details on the stochastic simulations which we have carried out to corroborate our analytic approach. The central result of this work is then addressed in Sec. VI, where two-dimensional analytic phase diagrams are investigated. Lines of continuous and discontinuous phase transitions appear and induce a variety of multicritical points at their intersection. A brief summary and outlook concludes this work.

II. THE MODEL

In this section, we describe our model in terms of spin transport as well as two-lane traffic. Though we will preferentially use the language of spins in the subsequent sections, the two-lane interpretation is of no lesser interest, and straightforwardly obtained. Furthermore, we introduce two symmetries which are manifest on the level of the dynamical rules.

1. Dynamical rules

We consider hopping transport on a one-dimensional lattice, composed of L sites, with open boundaries, see Fig. 1. Particles possess internal states, which we restrict to two different kinds; adopting a spin notation, they are referred to as spin-up (\uparrow) and spin-down (\downarrow). They enter at the left boundary at rates α^\uparrow resp. α^\downarrow , and move unidirectionally from left to the right through the lattice. The timescale is fixed by putting the rate for these hopping events to unity. Within the bulk, particles may also flip their spin state, from spin-up to spin-down and back, at rate ω . Finally, having reached the right boundary, particles may exit the system at rates β^\uparrow resp. β^\downarrow , depending on their spin state. We allow all of these processes only under the constraint of Pauli's exclusion principle, meaning that every lattice site may at most be occupied by one particle of a given state. Spin-up and spin-down thus may simultaneously occupy the same site, however two particles with identical spin polarization cannot share a lattice site. In summary, our dynamical rules are the following:

- (i) at site $i = 1$ (left boundary), particles with spin-up (spin-down) may enter at rate α^\uparrow (α^\downarrow)
- (ii) at site $i = L$ (right boundary), particles with spin-up (spin-down) leave the lattice at rate β^\uparrow (β^\downarrow)
- (iii) particles may hop at unit rate from site $i - 1$ to the neighboring site i for $i \in \{2, \dots, L\}$, i.e. within bulk
- (iv) within bulk, particles can flip their spin state with rate ω , i.e. spin-up turns into spin-down and vice versa

always respecting Pauli's exclusion principle. Processes (i) to (iii) constitute the Totally Asymmetric Simple Exclusion Processes (TASEP) for the two different states separately, while rule (iv) induces a coupling between them. Indeed, when the spin flip rate ω vanishes, we recover the trivial situation of two independent TASEPs, while we will show that a proper treatment of ω through a mesoscopic scaling induces nontrivial effects.

2. Two-lane interpretation

Having introduced our model in the language of semi-classical spin transport, where Pauli's exclusion principle is respected while phase coherence completely ignored, we now want to show that it also describes transport with site exclusion on two parallel lanes. As schematically drawn in Fig. 2, we consider two parallel lanes, each consisting of L sites, labeled as upper lane (I) and lower lane (II). They are identified with the internal states of the particles considered before: a particle with spin-up (spin-down) now corresponds to a particle on lane I (lane II). The processes (i) and (ii) describe entering of particles at lane I (II) at rate $\alpha^I \equiv \alpha^\uparrow$ ($\alpha^{II} \equiv \alpha^\downarrow$) and exiting of lane I (II) at rate $\beta^I \equiv \beta^\uparrow$ ($\beta^{II} \equiv \beta^\downarrow$). Due to (iii), particles hop unidirectionally to the right on each individual lane; at rate ω , they may switch from lane I to II and back. Pauli's exclusion principle translates into simple site exclusion: all the above processes are allowed under the constraint of admitting at most one particle per site. Again, we clearly observe that it is process (iv) that couples two TASEPs, namely the ones on each individual lane, to each other.

3. Symmetries

Already on the level of the dynamical rules (i)-(iv) presented above, two symmetries are manifest that will prove helpful in the analysis of the system's behavior. We refer to the absence of particles with certain state as holes with the opposite respective state [35]. Considering their motion, we observe that the dynamics of the holes is governed by the identical rules (i) to (iv), with "left" and "right" interchanged, i.e. with a discrete transformation

of sites $i \leftrightarrow L - i$ as well as rates $\alpha^{\uparrow,\downarrow} \leftrightarrow \beta^{\downarrow,\uparrow}$. The system thus exhibits a *particle-hole symmetry*. Even more intuitively, the two states behave qualitatively identical. Indeed, the system remains invariant upon changing spin-up to spin-down states and vice versa with a simultaneous interchange of $\alpha^\uparrow \leftrightarrow \alpha^\downarrow$ and $\beta^\uparrow \leftrightarrow \beta^\downarrow$, constituting a *spin symmetry* (in terms of the two-lane interpretation, it translates into a *lane symmetry*).

When analyzing the system's behavior in the five-dimensional phase space, constituted of the entrance and exit rates $\alpha^{\uparrow,\downarrow}$, $\beta^{\uparrow,\downarrow}$ and ω , these symmetries allow to connect different regions in phase space, and along the way to simplify the discussion.

III. MEAN-FIELD EQUATIONS, CURRENTS, AND THE CONTINUUM LIMIT

In this section, we shall make use the dynamical rules introduced above to set up a quantitative description for the densities and currents in the system. Within a mean-field approximation, their time evolution is expressed through one-point functions only, namely the average occupations of a lattice site. We focus on the properties of the non-equilibrium steady state, which results from boundary processes (entering and exiting events) as well as bulk ones (hopping and spin flip events). Both types of processes compete if their time-scales are comparable; we ensure this condition by introducing a *mesoscopic scaling* for the spin flip rate ω . Our focus is on the limit of large system sizes L , which is expected to single out distinct phases. To solve the resulting equations for the densities and currents, a continuum limit is then justified, and it suffices to consider the leading order in the small parameter, viz. the ratio of the lattice constant to system size. Such an approach has been successfully introduced in [29, 30] in the context of TASEP coupled to Langmuir dynamics.

A. Mean field approximation and currents

Let $n_i^\uparrow(t)$ resp. $n_i^\downarrow(t)$ be the fluctuating occupation number of site i for spin-up resp. spin-down state, i.e. $n_i^{\uparrow,\downarrow}(t) = 1$ if this site is occupied at time t by a particle with the specified spin state and $n_i^{\uparrow,\downarrow}(t) = 0$ otherwise. Performing ensemble averages, the expected occupation, denoted by $\rho_i^\uparrow(t)$ and $\rho_i^\downarrow(t)$, is obtained. Within a mean-field approximation, higher order correlations between the occupation numbers are neglected, i.e. we impose

$$\langle n_i^r(t) n_j^s(t) \rangle = \rho_i^r(t) \rho_j^s(t); \quad r, s \in \{\uparrow, \downarrow\}. \quad (1)$$

Equations of motion for the densities can be obtained via *balance equations*: The time-change of the density at a certain site is related to appropriate currents. The spatially varying *spin current* $j_i^\uparrow(t)$ quantifies the rate

at which particles of spin state \uparrow at site $i-1$ hop to the neighboring site i . Within the mean-field approximation, Eq. (1), the current is expressed in terms of densities

$$j_i^\uparrow(t) = \rho_{i-1}^\uparrow(t)[1 - \rho_i^\downarrow(t)], \quad i \in \{2, \dots, L\}, \quad (2)$$

and similarly for the current $j_i^\downarrow(t)$. The sum yields the total *particle current* $J_i(t) \equiv j_i^\uparrow(t) + j_i^\downarrow(t)$. Due to the spin flip process (iv), there also exists a leakage current $j_i^{\uparrow\downarrow}(t)$ from spin-up state to spin-down state. Within mean-field

$$j_i^{\uparrow\downarrow}(t) = \omega \rho_i^\uparrow(t)[1 - \rho_i^\downarrow(t)], \quad (3)$$

and similarly for the current $j_i^{\downarrow\uparrow}(t)$ from spin-down to spin-up state. Now, for $i \in \{2, \dots, L-1\}$ we can use balance equations to obtain the time evolution of the densities,

$$\frac{d}{dt} \rho_i^\uparrow(t) = j_i^\uparrow(t) - j_{i+1}^\uparrow(t) + j_i^{\downarrow\uparrow}(t) - j_i^{\uparrow\downarrow}(t). \quad (4)$$

This constitutes an exact relation. Together with the mean field approximation for the currents, Eqs. (2, 3), one obtains a set of closed equations for the local densities

$$\begin{aligned} \frac{d}{dt} \rho_i^\uparrow(t) = & \rho_{i-1}^\uparrow(t)[1 - \rho_i^\uparrow(t)] - \rho_i^\uparrow(t)[1 - \rho_{i+1}^\uparrow(t)] \\ & + \omega \rho_i^\downarrow(t) - \omega \rho_i^\uparrow(t). \end{aligned} \quad (5)$$

At the boundary of the track, the corresponding expressions involve also the entrance and exit events, which are treated again in the spirit of a mean-field approach

$$\begin{aligned} \frac{d}{dt} \rho_1^\uparrow(t) = & \alpha^\uparrow[1 - \rho_1^\uparrow(t)] - \rho_1^\uparrow(t)[1 - \rho_2^\uparrow(t)] \\ & + \omega \rho_1^\downarrow(t) - \omega \rho_1^\uparrow(t), \end{aligned} \quad (6)$$

$$\begin{aligned} \frac{d}{dt} \rho_L^\uparrow(t) = & \rho_{L-1}^\uparrow(t)[1 - \rho_L^\uparrow(t)] - \beta^\uparrow \rho_L^\uparrow(t) \\ & + \omega \rho_L^\downarrow(t) - \omega \rho_L^\uparrow(t). \end{aligned} \quad (7)$$

Due to the spin symmetry, i.e. interchanging \uparrow and \downarrow , an analogous set of equations for the time evolution of the density of particles with spin-down state holds.

In the stationary state, the densities $\rho_i^{\uparrow(\downarrow)}(t)$ do not depend on time t , such that the time derivatives in Eqs. (5)-(7) vanish. Therefrom, we immediately derive the spatial conservation of the particle current: Indeed, summing Eq. (4) with the corresponding equation for the density of spin-down states yields

$$J_i = J_{i+1}, \quad i \in \{2, \dots, L-1\}, \quad (8)$$

such that the particle current does not depend on the spatial position i . Note that this does not apply to the individual spin currents, they *do* have a spatial dependence arising from the leakage currents.

In a qualitative discussion, let us now anticipate the effects that arise from the non-conserved individual spin currents as well as from the conserved particle current. The latter has its analogy in TASEP, where the particle current is spatially conserved as well. It leads to two distinct regions in the parameter space: one where the current is determined by the left boundary, and the other where it is controlled by the right one. Both regions are connected by the discrete particle-hole symmetry. Thus, in general, discontinuous phase transitions arise when crossing the border from one region to the other. In our model, we will find similar behavior: the particle current is either determined by the left or by the right boundary. Again, both regions are connected by the discrete particle-hole symmetry, such that we expect discontinuous phase transitions at the border between both. Except for a small, particular region in the parameter space, this behavior is captured quantitatively by the mean-field approach and the subsequent analysis and is corroborated by stochastic simulations. The phenomena linked to the particular region will be presented elsewhere [31].

On the other hand, the non-conserved spin currents may be compared to the current in TASEP coupled to Langmuir kinetics, see [29, 30]. Due to attachment and detachment processes, the in-lane current is only weakly conserved, allowing for a novel phenomena, namely phase separation into a low-density and a high-density region separated by a localized domain wall. The transitions to this phase are continuous considering the domain wall position x_w as the order parameter. In our model, an analogous but even more intriguing phase will appear as well, with continuous transitions being possible.

B. Mesoscopic scaling and the continuum limit

1. Mesoscopic scaling

Phases and corresponding phase transitions are expected to emerge in the limit of large system size, $L \rightarrow \infty$, which therefore constitutes the focus of this work. We expect interesting phase behavior to arise from the coupling of spin-up and spin-down states via spin flip events, in addition to the entrance and exit processes. Clearly, if spin flips occur on a fast time-scale, comparable to the hopping events, the spin degree of freedom is relaxed, such that the system's behavior is effectively the one of a TASEP. Previous work on related two-lane models [26, 27] focused on the physics in that situation. In this work, we want to highlight the dynamical regime where coupling through spin flips is present, however not sufficiently strong to relax the system's internal degree of freedom. In other words, we consider physical situations where spin flips occur on the same time-scale as the entrance/exit processes. Defining the *gross* spin flip rate $\Omega = \omega L$ yields a measure of how often a particle flips its spin state while traversing the system. To ensure competition between spin flips with boundary processes,

a *mesoscopic scaling* of the rate ω is employed by keeping Ω fixed, of the same order as the entrance/exit rates, when the number of lattice sites becomes large $L \rightarrow \infty$.

2. Continuum limit and first order approximation

The total length of the lattice will be fixed to unity and one may define consistently the lattice constant $\epsilon = 1/L$. In the limit of large systems $\epsilon \rightarrow 0$, a *continuum limit* is anticipated. We introduce continuous functions $\rho^\uparrow(x)$ resp. $\rho^\downarrow(x)$ through $\rho^\uparrow(x_i) = \rho_i^\uparrow$ resp. $\rho^\downarrow(x_i) = \rho_i^\downarrow$ at the discrete points $x_i = i\epsilon$. Expanding these to first order in the lattice constant:

$$\rho^{\uparrow(\downarrow)}(x_{i\pm 1}) = \rho^{\uparrow(\downarrow)}(x_i \pm \epsilon) = \rho^{\uparrow(\downarrow)}(x_i) \pm \epsilon \partial_x \rho^{\uparrow(\downarrow)}(x_i), \quad (9)$$

the difference equations (5)-(7) turn into differential equations. Observing that $\omega = \epsilon\Omega$ is already of order ϵ , we find that the zeroth order of Eq. (5) vanishes, and the first order in ϵ yields

$$[2\rho^\uparrow(x) - 1]\partial_x \rho^\uparrow(x) + \Omega\rho^\downarrow(x) - \Omega\rho^\uparrow(x) = 0. \quad (10)$$

Similarly, the same manipulations for ρ^\downarrow yield

$$[2\rho^\downarrow(x) - 1]\partial_x \rho^\downarrow(x) + \Omega\rho^\uparrow(x) - \Omega\rho^\downarrow(x) = 0. \quad (11)$$

The expansion of Eqs. (6) and (7) in powers of ϵ , yields in zeroth order

$$\begin{aligned} \rho^\uparrow(0) &= \alpha^\uparrow, & \rho^\uparrow(1) &= 1 - \beta^\uparrow, \\ \rho^\downarrow(0) &= \alpha^\downarrow, & \rho^\downarrow(1) &= 1 - \beta^\downarrow, \end{aligned} \quad (12)$$

which impose *boundary conditions*. Since two boundary conditions are enough to specify a solution of the coupled first order differential equations, the system is apparently over-determined. We expect the full analytic solution, i.e. where all orders in ϵ are incorporated, to be only *piecewise* given by the first-order approximation, Eqs. (10)-(12). Between these branches, the solution will depend on higher orders of ϵ , therefore, these intermediate regions scale with order ϵ and higher. They vanish in the limit of large systems, $\epsilon \rightarrow 0$, yielding *domain walls* or *boundary layers*.

Let us explain the latter terms. At the position of a domain wall, situated in bulk, the density changes discontinuously its value, from one of a low-density region to one of a high-density one. Boundary layers are pinned to the boundaries of the system, there as well, the density changes discontinuously: from a value that is given by the boundary condition to that of a low-density or high-density region.

3. Symmetries and currents revisited

In the following, we reflect important properties of the system, symmetries and currents, on the level of the first-order approximation, Eqs. (10)-(12). The explicit solution of the latter can be found in Appendix A.

The particle-hole symmetry, already inferred from the dynamical rules, now takes the form

$$\begin{aligned} \rho^{\uparrow(\downarrow)}(x) &\leftrightarrow 1 - \rho^{\uparrow(\downarrow)}(1 - x), \\ \alpha^{\uparrow(\downarrow)} &\leftrightarrow \beta^{\uparrow(\downarrow)}. \end{aligned} \quad (13)$$

Interchanging \uparrow and \downarrow in the densities as well as the in- and outgoing rates yields the spin symmetry,

$$\begin{aligned} \rho^\uparrow(x) &\leftrightarrow \rho^\downarrow(x), \\ \alpha^\uparrow &\leftrightarrow \alpha^\downarrow, \\ \beta^\uparrow &\leftrightarrow \beta^\downarrow. \end{aligned} \quad (14)$$

The individual spin currents as well as the particle current have been anticipated to provide further understanding of the system's behavior. In the continuum limit the zeroth order of the spin currents is found to be $j^{\uparrow(\downarrow)}(x) = \rho^{\uparrow(\downarrow)}(x)[1 - \rho^{\uparrow(\downarrow)}(x)]$, such that Eqs. (10), (11) may be written in the form

$$\partial_x j^\uparrow = \Omega[\rho^\downarrow - \rho^\uparrow], \quad \partial_x j^\downarrow = \Omega[\rho^\uparrow - \rho^\downarrow]. \quad (15)$$

The terms on the right-hand side, arising from the spin flip process (iv), are seen to violate the spatial conservation of the spin currents. However, due to the mesoscopic scaling of the spin flip rate ω , the leakage currents between the spin states are only weak, see Eq. (3), locally tending to zero when $\epsilon \rightarrow 0$, such that the spin currents vary *continuously* in space. This finding imposes a condition for the transition from one branch of first-order solution to another, as described above: such a transition is only allowed when the corresponding spin currents are continuous at the transition point, thus singling out distinct positions for a possible transition.

Finally, summing the two equations in Eq. (15) yields the spatial conservation of the particle current: $\partial_x J = 0$.

IV. PARTITION OF THE PARAMETER SPACE AND THE GENERIC DENSITY BEHAVIOR

In this section, we partition the five-dimensional parameter space, spanned by $\alpha^{\uparrow,\downarrow}$, $\beta^{\uparrow,\downarrow}$, Ω , into three distinct regions: the maximal-current region (MC), the injection-limited (IN) and the extraction-limited one (EX). While trivial phase behavior occurs in the MC region, our focus is on the IN and EX region, (connected by particle-hole symmetry), where a striking polarization phenomenon occurs. The generic phase behavior in these regions is derived, exhibiting this effect.

A. Effective rates

The entrance and exit rates as well as the carrying capacity of the bulk impose restrictions on the particle current. The capacity of the bulk bounds the individual spin currents by maximal values of 1/4, occurring for a

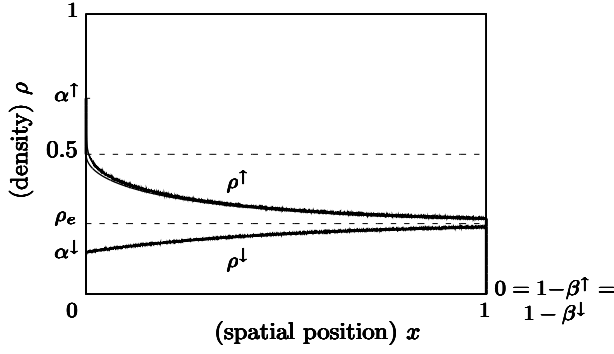


FIG. 3: Illustration of the effective rates. The right boundary is “open”, such that only the capacity of the bulk and the entrance rates limit the spin currents. The injection rate $\alpha^\uparrow > \frac{1}{2}$ effectively acts as $\frac{1}{2}$. The analytic predictions correspond to the solid lines, the results from stochastic simulations for $L = 10000$ are indicated by the wiggly line. With increasing spatial position, the densities approach a common value ρ_e . The parameters used are $\alpha^\uparrow = 0.7$, $\alpha^\downarrow = 0.15$, $\Omega = 0.5$.

respective density of $1/2$, as seen from the previous result $j^{\uparrow(\downarrow)} = \rho^{\uparrow(\downarrow)}[1 - \rho^{\uparrow(\downarrow)}]$, which holds to lowest order in the lattice constant ϵ . To illustrate the influence of the injection and extraction rates, we first consider the case where the right boundary is completely “open”, i.e. $\beta^\uparrow = \beta^\downarrow = 1$. Particles then leave the system unhindered, such that only the entrance rates limit the particle current. Provided one of these rates, say α^\uparrow , exceeds the value $1/2$, the current of the corresponding state (\uparrow) is limited by the capacity of the bulk to a value of $1/4$ in the vicinity of the left boundary (it may decrease with increasing spatial position due to the coupling to the other state). A boundary layer thus forms in the density profile of spin-up state at the left boundary, connecting the value of the injection rate α^\uparrow to the value $1/2$, which corresponds to the maximal spin current $1/4$. Up to this boundary layer, the density profile $\rho^\uparrow(x)$ is identical to the one where α^\uparrow takes a value of $1/2$, c.f. Fig. 3. Similar reasoning holds for the extraction rates $\beta^{\uparrow(\downarrow)}$, they as well behave effectively as $1/2$ when exceeding this value. To treat these findings properly, we introduce the *effective rates*

$$\alpha_{\text{eff}}^{\uparrow(\downarrow)} = \min\left[\alpha^{\uparrow(\downarrow)}, \frac{1}{2}\right], \quad (16a)$$

$$\beta_{\text{eff}}^{\uparrow(\downarrow)} = \min\left[\beta^{\uparrow(\downarrow)}, \frac{1}{2}\right]. \quad (16b)$$

The system’s bulk behavior will only depend on them, and, in particular, remain unaffected when a rate is varied at values exceeding $1/2$.

B. Injection-limited, extraction-limited, and maximal current region

Equipped with these results, in the case of an “open” right boundary, the spin currents in the vicinity of the

left boundary are given by $j^\uparrow = \alpha_{\text{eff}}^\uparrow(1 - \alpha_{\text{eff}}^\uparrow)$ resp. $j^\downarrow = \alpha_{\text{eff}}^\downarrow(1 - \alpha_{\text{eff}}^\downarrow)$, resulting in a particle current J_{IN} imposed by the injection rates: $J_{\text{IN}} = \alpha_{\text{eff}}^\uparrow(1 - \alpha_{\text{eff}}^\uparrow) + \alpha_{\text{eff}}^\downarrow(1 - \alpha_{\text{eff}}^\downarrow)$. The analogous relations, with the injection and extraction rates interchanged, hold for the case of an “open” left boundary, $\alpha^\uparrow = \alpha^\downarrow = 1$, the particle current is then controlled by the right boundary: $J_{\text{EX}} = \beta_{\text{eff}}^\uparrow(1 - \beta_{\text{eff}}^\uparrow) + \beta_{\text{eff}}^\downarrow(1 - \beta_{\text{eff}}^\downarrow)$. In general, depending on which imposes the stronger restriction, either the left or the right boundary limits the particle current: $J \leq \min(J_{\text{IN}}, J_{\text{EX}})$ (indeed, $J = \min(J_{\text{IN}}, J_{\text{EX}})$ holds except for an anomalous situation, where the current is lower than this value [36]). Depending on which of both cases applies, two complementary regions in phase space are distinguished: $J_{\text{IN}} < J_{\text{EX}}$ is termed *injection-limited region* (IN), while $J_{\text{IN}} > J_{\text{EX}}$ defines the *extraction-limited region* (EX). Since they are connected by discrete particle-hole symmetry, we expect *discontinuous phase transitions* across the border between both, to be referred as *IN-EX boundary*. At the latter, the system is in a coexistence of both neighboring phases; we will now argue how this is manifested in the emergence of (delocalized) domain walls in the density profiles of *both* individual states (see also [31] for a detailed discussion). Indeed, when a domain wall appears, it interpolates between a piece of first-order solution, fulfilling the left boundary condition, and another piece obeying the right boundary condition. If domain walls simultaneously occur for spin-up and spin-down state, the particle current at the left boundary is given by J_{IN} , and at the right by J_{EX} . Being conserved, this situation is possible only for $J = J_{\text{IN}} = J_{\text{EX}}$:

$$\begin{aligned} \alpha_{\text{eff}}^\uparrow(1 - \alpha_{\text{eff}}^\uparrow) + \alpha_{\text{eff}}^\downarrow(1 - \alpha_{\text{eff}}^\downarrow) &= \\ &= \beta_{\text{eff}}^\uparrow(1 - \beta_{\text{eff}}^\uparrow) + \beta_{\text{eff}}^\downarrow(1 - \beta_{\text{eff}}^\downarrow). \end{aligned} \quad (17)$$

For $J < 1/2$ this condition describes the submanifold of the IN-EX boundary.

When both entrance rates α^\uparrow , α^\downarrow as well as both exit rates β^\uparrow , β^\downarrow exceed the value $1/2$, the particle current is limited by neither boundary, but only through the carrying capacity of the bulk, restricting it to twice the maximal value $1/4$ of the individual spin currents: $J = 1/2$. The latter situation therefore constitutes the *maximal current region* (MC).

C. The generic state of the densities

In this subsection, we derive the generic state of the density profiles. Considering different positions of the localized domain wall that will emerge and applying particle-hole as well as spin symmetry to this state, yields all possible phases.

Simple phase behavior occurs in the MC region: up to boundary layers, the densities remain constant at values $1/2$, yielding the maximal particle current $J = 1/2$.

This is in contrast to the striking phenomena emerging in the IN as well as the EX region, which are investigated in the following. In the previous subsection, we have argued that two simultaneous domain walls for the spin-resolved densities are possible only on the submanifold of the IN-EX boundary. Accordingly, within the IN or EX region, at least one boundary layer has to occur; we consider the case that it arises for the spin-down state, the other situation is obtained from spin symmetry. We shall demonstrate in the following, that a domain wall for the spin-up state may emerge in extended regions of the phase diagram. Such a behavior then constitutes a coexistence of phases, characterized by phase separation. In this scenario the spin-up density profile close to the left is determined by the solution of the first order differential equation obeying the left boundary condition $\rho^\uparrow(x=0) = \alpha_{\text{eff}}^\uparrow$. Similarly near the right boundary the profile is determined by the solution that fulfills the right boundary condition: $\rho^\uparrow(x=1) = 1 - \beta_{\text{eff}}^\uparrow$. Somewhere in bulk, the solutions have to be concatenated; generically this cannot be achieved smoothly, the spin-up density profile exhibits a jump in bulk and a domain wall forms. To complete the generic picture assume that the boundary for the spin-down density is pinned to the right end. Consequently the current in bulk is determined by the injection rates, $J = J_{\text{IN}}$, which defined the IN region. Similarly, for a boundary layer at the left, the current is limited by extraction processes, $J = J_{\text{EX}}$ characteristic for the EX region.

Figure 4(a) exemplifies the generic density profile, and results from stochastic simulations (detailed in the next section) are compared to analytic findings. Approaching the mesoscopic limit by increasing the system sizes, singles out the analytic prediction. In the vicinity of the left boundary, the densities follow the first-order solution (named $\rho_l^\uparrow, \rho_l^\downarrow$) with the left boundary conditions $\rho_l^{\uparrow(\downarrow)}(x=0) = \alpha_{\text{eff}}^{\uparrow(\downarrow)}$. Then, at a position x_w , the density of spin-up states exhibits a discontinuity: to the right of x_w , the densities are given by another piece of first-order solution (named $\rho_r^\uparrow, \rho_r^\downarrow$). The latter satisfies $\rho_r^\uparrow(x=1) = 1 - \beta_{\text{eff}}^\uparrow$, and $\rho_r^\downarrow(x=1)$ is found from the conservation of the particle current:

$$\begin{aligned} J &= \alpha_{\text{eff}}^\uparrow(1 - \alpha_{\text{eff}}^\uparrow) + \alpha_{\text{eff}}^\downarrow(1 - \alpha_{\text{eff}}^\downarrow) \\ &= \beta_{\text{eff}}^\uparrow(1 - \beta_{\text{eff}}^\uparrow) + \rho_r^\downarrow(x=1)[1 - \rho_r^\downarrow(x=1)]. \end{aligned} \quad (18)$$

The precise value β^\downarrow is irrelevant for the phase behavior as long as the phases are given as in Fig. 4. Merely the height and detailed shape of the boundary layer in the spin-down states is affected by β^\downarrow .

To determine the position x_w of the domain wall arising for spin-up states, we use the continuity of the spin currents, see Fig. 4(b). Indeed, though they are not spatially conserved, the mesoscopic scaling of the spin flip rate ω was seen to cause a only slowly varying spatial dependence; in the continuum limit, the spin currents are continuous. This condition singles out a distinct spatial position for the domain wall: Denote by $\rho_l^\uparrow(x_w)$ the

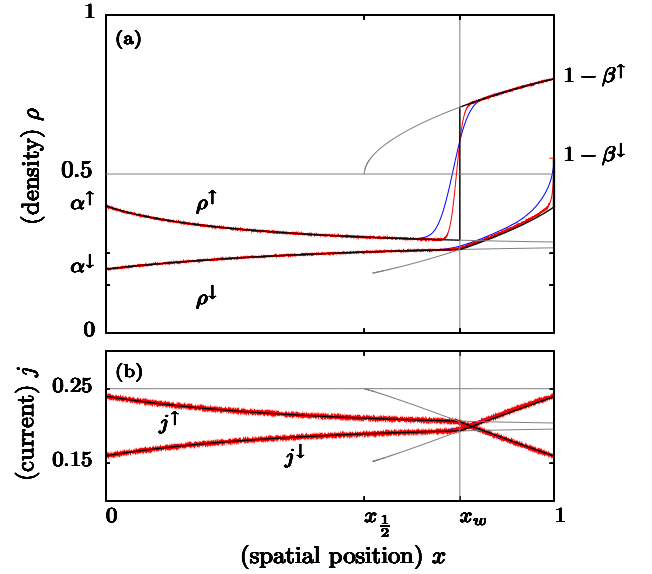


FIG. 4: (Color online) The densities (a) and currents (b) in the IN region: generic state, exhibiting the polarization phenomenon. Results from stochastic simulations are shown as blue ($L = 2000$) resp. red ($L = 10000$) lines. They piecewise obey the first order approximations (black), grey lines indicate continuations of the latter into regions where the densities are no longer given by them. The parameters are $\alpha^\uparrow = 0.4$, $\alpha^\downarrow = 0.2$, $\beta^\uparrow = 0.2$, $\beta^\downarrow = 0.45$, and $\Omega = 0.5$.

value of the density to the left of x_w , and $\rho_r^\uparrow(x_w)$ the value to the right. From $j^\uparrow = \rho^\uparrow(1 - \rho^\uparrow)$ together with $\rho_l^\uparrow(x_w) \neq \rho_r^\uparrow(x_w)$, we arrive at the condition

$$\rho_l^\uparrow(x_w) = 1 - \rho_r^\uparrow(x_w) \quad (19)$$

for the domain wall position. For TASEP-like transport the particle-hole symmetry restricts the density jump to this mirror relation. More general current-density relation are feasible [32, 33], but are not expected to change the picture qualitatively.

When considering the internal states as actual spins, the appearance of a domain wall in the density profile of one of the spin states results in a *spontaneous polarization phenomenon*. Indeed, while both the density of spin-up and spin-down remain at comparable low values in the vicinity of the left boundary, this situation changes upon crossing the point x_w . There, the density of spin-up jumps to a high value, while the one of spin-down remains at a low one, resulting in a polarization in this region.

Comparing the generic phase behavior to the one of TASEP, we observe that the IN region can be seen as the analogue to the low-density region there: within both, a low-density phase accompanied by a boundary layer at the right boundary arises. Following these lines, the EX region has its analogue in the high-density region, while the MC region is straightforwardly generalized from the one of TASEP. Furthermore, the delocalization transition

across the IN-EX boundary is similar to the appearance of a delocalized domain wall at the coexistence line in TASEP.

D. Phases and phase boundaries

In the generic situation of Fig. 4, the density of spin-down is in a homogeneous low-density (LD) state, while for spin-up, a low-density and a high-density region coexist. We refer to the latter as the LD-HD_{IN} phase, as the phase separation arises within the IN region, to be contrasted from a LD-HD_{EX} phase which may arise within the EX region. Clearly, the LD-HD_{IN} phase is only present if the position x_w of the domain wall lies within bulk; tuning the system's parameter, it may leave the system through the left or right boundary, resulting in a homogeneous phase. Indeed, $x_w = 1$ marks the transition between the LD-HD_{IN} phase and the pure LD state, while at $x_w = 0$ the density changes from the LD-HD_{IN} to a homogeneous high-density (HD) state. Regarding the domain wall position x_w as an order parameter, these transitions are continuous. Implicit analytic expressions for these phase boundaries, derived in the following, are obtained from the first-order approximation.

Spin symmetry yields the analogous situation with a domain wall appearing in the density profile of spin-down, while particle-hole symmetry maps it to the EX region, where a pure HD phase arises for one of the spins. Discontinuous transitions accompanied by delocalized domain walls appear at the submanifold of the IN-EX boundary (see [31] for a detailed discussion).

The phase boundaries may be computed from the condition $x_w = 0$ and $x_w = 1$ in the situation of Fig. 4. Consider first the case of $x_w = 0$. There, the density profiles are completely given by the first-order approximation $\rho_r^{\uparrow(\downarrow)}$ satisfying the boundary conditions at the right. The condition (19) translates to

$$\rho_r^{\uparrow}(x=0) = 1 - \rho_l^{\uparrow}(x=0) = 1 - \alpha_{\text{eff}}^{\uparrow} \quad (20)$$

which yields an additional constraint on the system's parameters, defining the hyper-surface in the IN region where $x_w = 0$ occurs and thus the phase boundary between the LD-HD_{IN} and the pure HD phase. Similarly, if $x_w = 1$, the densities follow the left solution $\rho_l^{\uparrow(\downarrow)}(x)$, determined by the left boundary conditions, within the whole system. From (19) we obtain

$$\rho_l^{\uparrow}(x=1) = 1 - \rho_r^{\uparrow}(x=1) = \beta_{\text{eff}}^{\uparrow}. \quad (21)$$

Again, the latter is a constraint on the parameters and defines the hyper-surface in the IN region where $x_w = 1$ is found, being the phase boundary between the LD-HD_{IN} and the homogeneous LD phase.

The conditions (20), (21) yield implicit equations for the phase boundaries, the phase diagram is thus determined up to solving algebraic equations, which may

be achieved numerically. Further insight concerning the phase boundaries are possible and may be obtained analytically, which we discuss in the following.

First, we find a submanifold in parameter space that, for all values of the rate Ω , lies entirely in the manifold of the phase boundary defined by $x_w = 1$. Indeed for the case where the density profile for spin-down is constant (except for the boundary layer at the right) and less than a half, Eqs. (10,11, 12) are fulfilled for $\alpha^{\uparrow} = \alpha^{\downarrow} = \beta^{\uparrow} < 1/2$ within the IN region, irrespective of the value of Ω .

Second, we investigate the phase boundary determined by $x_w = 0$. Comparing with Fig. 4, we observe that the first-order approximation ρ_r^{\uparrow} for the density of spin-up may reach the value $\frac{1}{2}$ at a point which is denoted by $x_{\frac{1}{2}}$: $\rho_r^{\uparrow}(x_{\frac{1}{2}}) = \frac{1}{2}$. This point corresponds to a branching point of the first-order solution; studying it, we observe that $x_{\frac{1}{2}}$ increases for increasing value of the rate Ω . The domain wall in the density of spin-up can only emerge at a value $x_w \geq x_{\frac{1}{2}}$, at most, $x_w = x_{\frac{1}{2}}$, in which case a domain wall with infinitesimal small height arises. Concerning the phase boundary specified by $x_w = 0$, it only exists as long as $x_{\frac{1}{2}} \leq 0$, and the case $x_w = x_{\frac{1}{2}} = 0$ corresponds to a domain wall of infinitesimal height, which is only feasible if $\alpha_{\text{eff}}^{\uparrow} = \frac{1}{2}$. Now, for given rates $\alpha_{\text{eff}}^{\uparrow} = \frac{1}{2}$, α^{\downarrow} , β^{\uparrow} , the condition $x_{\frac{1}{2}} = 0$ yields a critical rate $\Omega^*(\alpha^{\downarrow}, \beta^{\uparrow})$, depending on the rates $\alpha^{\downarrow}, \beta^{\uparrow}$. The situation $x_w = 0$ can only emerge for rates $\Omega \leq \Omega^*(\alpha^{\downarrow}, \beta^{\uparrow})$. Varying the rates α^{\uparrow} , α^{\downarrow} and β^{\uparrow} , the critical rate $\Omega^*(\alpha^{\downarrow}, \beta^{\uparrow})$ changes as well. In App. A, we show that its largest value occurs at $\alpha^{\downarrow} = \beta^{\uparrow} = 0$. They yield the rate $\Omega_C \equiv \Omega^*(\alpha^{\downarrow} = \beta^{\uparrow} = 0)$, which is calculated to be

$$\Omega_C = 1 + \frac{1}{4}\sqrt{2} \ln(3 - 2\sqrt{2}) \approx 0.38. \quad (22)$$

The critical $\Omega^*(\alpha^{\downarrow}, \beta^{\uparrow})$ are thus lying in the interval between 0 and Ω_C : $\Omega^*(\alpha^{\downarrow}, \beta^{\uparrow}) \in [0, \Omega_C]$, and all values in this interval in fact occur. The rate Ω_C defines a scale in the spin-flip rate rate Ω : For $\Omega \leq \Omega_C$, the phase boundary determined by $x_w = 0$ exists, while disappearing for $\Omega > \Omega_C$.

Third, we study the form of the phase boundaries for large Ω , meaning $\Omega \gg \Omega_C$ such that the phase boundary specified by $x_w = 0$ leads to unphysical parameters. It turns out that in this situation, for the left solution, the densities quickly approximate a common value ρ_e . The latter is found from conservation of the particle current: $2\rho_e(1 - \rho_e) = J$. We now consider the implications for the phase boundary determined by $x_w = 1$. With $\rho_l^{\uparrow}(x=1) = \rho_e$, Eq. (21) turns into $\rho_e = \beta_{\text{eff}}^{\uparrow}$, yielding

$$2\beta_{\text{eff}}^{\uparrow}(1 - \beta_{\text{eff}}^{\uparrow}) = \alpha_{\text{eff}}^{\uparrow}(1 - \alpha_{\text{eff}}^{\uparrow}) + \alpha_{\text{eff}}^{\downarrow}(1 - \alpha_{\text{eff}}^{\downarrow}). \quad (23)$$

The hyper-surface specified by this equation is, for large Ω , asymptotically approached by the phase boundary between the LD-HD_{IN} and the LD phase. It constitutes a simple quadratic equation in the in- and outgoing rates, independent of β^{\downarrow} , and contains the set $\alpha^{\uparrow} = \alpha_{\text{eff}}^{\downarrow} = \beta^{\uparrow}$.

V. STOCHASTIC SIMULATIONS

To confirm our analytic findings from the previous section, we have performed stochastic simulations. The dynamical rules (i)-(iv) described in Subsec. II 1 were implemented using random sequential updating. In our simulations, we have performed averages over typically 10^5 time steps, with $10 \times L$ steps of updating between successive ones. Finite size scaling singles out the analytic solution in the limit of large system sizes, as exemplified in Fig. 3 and 4.

For all the simulations we have checked that the analytic predictions are recovered upon approaching the mesoscopic limit. We attribute the apparent exactness of our analytic approach in part to the exact current density relation in the steady state of TASEP [34]. The additional coupling of the two TASEPs in our model is only weak: the local exchange between the two states vanishes in the limit of large system sizes. Correlations between them are washed out, and mean-field is recovered.

The observed exactness of the analytic density profiles within the mesoscopic limit implies that our analytic approach yields exact phase diagrams as well. The latter are the subject of the subsequent section.

VI. TWO-DIMENSIONAL PHASE DIAGRAMS

In this section, we discuss the phase behavior on two-dimensional cuts in the whole five-dimensional parameter space. Already the simplified situation of equal injection rates, $\alpha^\uparrow = \alpha^\downarrow$, yields interesting behavior. There as well as in the general case, we investigate the role of the spin flip rate Ω by discussing the situation of small and large values of Ω .

A. Equal injection rates

In the situation of spin transport, when unpolarized particles are injected into the system, this translates into equal entrance rates, $\alpha^\uparrow = \alpha^\downarrow \equiv \alpha$. The appearance of a localized domain wall as depicted in Fig. 4 is then directly seen as a spontaneous polarization effect: while the densities of both spin states are *equal* in the vicinity of the left boundary unto the point x_w of the domain wall, a sudden difference emerges to the right of x_w . We thus encounter the polarization to jump from zero to a high value upon crossing x_w .

For the phase transitions emerging, the ones from LD to the LD-HD_{IN} arising in the IN region take a remarkably simple form. Their location is found from $x_w = 1$; when appearing in the density of spin-up states, it is determined by Eq. (21). Since $\rho^\uparrow(x) = \rho^\downarrow(x) = \alpha = \text{const.}$ for $x < x_w$, this condition turns into at $\alpha = \beta^\uparrow$. The latter transition line intersects the IN-EX boundary, given by Eq. (17), at $\beta^\uparrow = \beta^\downarrow = \alpha$, i.e. at the point where all entrance and exit rates coincide. At this *multicritical*

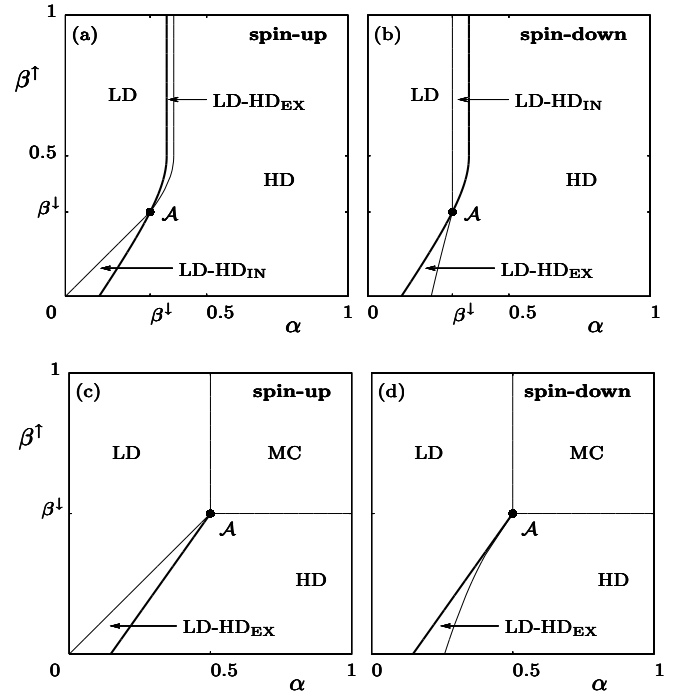


FIG. 5: Phase diagrams in the situation of equal entrance rates $\alpha^\uparrow = \alpha^\downarrow \equiv \alpha$ and large Ω . The phases of the densities of spin-up (spin-down) state are shown in (a) resp. (b) for a value $\beta^\downarrow = 0.3$. At a multicritical point \mathcal{A} , continuous lines (thin) intersect with a discontinuous line (bold), the IN-EX boundary. If $\beta^\downarrow \geq \frac{1}{2}$, the maximal current phase appears for spin-up, see (c), as well for spin-down, drawn in (d). In the first situation, the switching rate is $\Omega = 0.15$, while $\Omega = 0.2$ in the second.

point \mathcal{A} , a continuous line intersects a discontinuous one. The same transition in the density of spin-down state is, from similar arguments, located at $\alpha = \beta^\downarrow$, and also coincides with the IN-EX boundary in \mathcal{A} . Neither the multicritical point \mathcal{A} nor these phase boundaries depend on the magnitude of the gross spin flip rate Ω , i.e. qualitatively tuning the system's state is possible only upon changing the injection or extraction rates. The other phase transitions within the IN region, namely from the HD to the LD-HD_{IN} phase, are more involved. The analytic solution (A11), (A12) has to be considered together with the condition (20) for the transition. However, in the previous section, we have found that these transitions disappear for sufficiently large $\Omega > \Omega_C$.

1. Large values of Ω

We first consider the situation where neither phase transitions arising from $x_w = 0$ in the IN region nor from the analogue in the EX region do arise, which is guaranteed by $\Omega > \Omega_C$, but depending on the other parameters may also be fulfilled for smaller values of Ω . Having found the transitions within the IN region by simple expres-

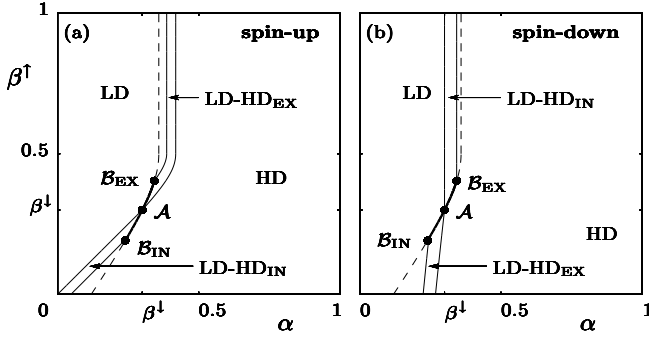


FIG. 6: Phase diagrams in the situation of Fig. 5 (a), (b), but with Ω changed to a small value, $\Omega = 0.05$. Additional phase transitions emerge in the IN as well as the EX region, accompanied by multicritical points \mathcal{B}_{IN} and \mathcal{B}_{EX} . Caused by them, phase transitions do no longer appear across some parts of the IN-EX boundary, which is there shown as dashed line.

sions, the ones emerging in the EX region are more complex and involve the full analytic solution (A11), (A12). Their most notable feature is that the width of the coexistence phase decreases with increasing spin flip rate Ω , until it finally vanishes in the limit $\Omega \rightarrow \infty$. This may be seen by considering the analogue of Eq. (23) in the EX region, which describes the phase boundary as it is asymptotically approached when $\Omega \rightarrow \infty$:

$$2\alpha_{\text{eff}}(1 - \alpha_{\text{eff}}) = \beta_{\text{eff}}^{\uparrow}(1 - \beta_{\text{eff}}^{\uparrow}) + \beta_{\text{eff}}^{\downarrow}(1 - \beta_{\text{eff}}^{\downarrow}); \quad (24)$$

it coincides with the IN-EX boundary.

We have drawn resulting phase diagrams in Fig. 5, showing the phase of spin-up (spin-down) in the left (right) panels, depending on α and β^{\uparrow} . Along the IN-EX boundary, being the same line (shown as bold) in the left and right panels, a delocalization transitions occur. At the multicritical point \mathcal{A} , it is intersected by continuous lines emerging within the IN resp. the EX region. When $\beta^{\downarrow} > 1/2$, a maximal current(MC) phase emerges in the upper right quadrant, see Fig. 5 (c)-(d).

2. Small values of Ω

When $\Omega < \Omega_C$, the appearance of additional phase transitions becomes possible. Within the IN region, the situation $x_w = 0$ may emerge, describing the transition from the HD to the LD-HD_{IN} phase; the analogue occurs in the EX region. Shown in Fig. 6, these lines intersect the IN-EX boundary at additional multicritical points \mathcal{B}_{IN} and \mathcal{B}_{EX} . Also, they partly substitute the IN-EX boundary as a phase boundary: across some parts of the latter, phase transitions do not arise. This behavior reflects the *decoupling* of the two states for decreasing spin flip rate Ω . Indeed, for $\Omega \rightarrow 0$, the states become more and more decoupled, such that the IN-EX boundary, involving the combined entrance and exit rates of both states, loses its significance.

3. Multicritical points

Although the shapes of most of the transition lines appearing in the phase diagrams shown in Fig. 6 are quite involved, they also exhibit simple behavior: *pair-wise*, namely one line from a transition in spin-up and another from a related transition in spin-down states, they intersect the IN-EX boundary in the same multicritical point. This intriguing phenomenon may be understood by considering the multicritical points: e.g., at \mathcal{A} , the transition line from the LD to the LD-HD_{IN} phase in the density profile of spin-up intersects the IN-EX boundary, which implies that there we have a domain wall in the density profile of spin-up at the position $x_w = 1$. However, being on the IN-EX boundary, Eq. (17) implies that in this situation a domain wall forms as well in the density of spin-down states, also located at $x_w = 1$, such that \mathcal{A} also marks the point where the transition line specified by $x_w = 1$ for spin-down states intersects the IN-EX boundary. Due to the special situation of equal entrance rates, one more pair of lines intersects in this point. Similarly, at \mathcal{B}_{IN} , the transition line from the HD to LD-HD_{IN} phase in the density profile of spin-up intersects the IN-EX boundary, such that a domain wall forms in the density of spin-up at $x_w = 0$. Again, as Eq. (17) holds on the IN-EX boundary, this implies the formation of a domain wall in the density of spin-down at $x_w = 1$, corresponding to the transition from the LD to the LD-HD_{EX} phase for spin-down in the EX region.

B. The general case

Having focused on the physically particularly enlightening case of equal entering rates in the previous subsection, we now turn to the general case. To illustrate our findings, we show phase diagrams depending on the injection and extraction rates for spin-up states, α^{\uparrow} and β^{\uparrow} . Similar behavior as for equal entrance rates is observed, the multicritical point \mathcal{A} now splits up into two distinct points \mathcal{A}_{IN} and \mathcal{A}_{EX} .

1. Large values of Ω : Asymptotic results

Again, large Ω prohibit the emergence of the phase transition from the HD to the LD-HD_{IN} phase in the IN region as well as from the LD to the LD-HD_{EX} phase within the EX region. In this paragraph, we consider phase diagrams which are approached asymptotically when $\Omega \rightarrow \infty$. Convergence is fast in Ω , and the asymptotic phase boundaries yield an excellent approximation already for $\Omega \gtrsim 2\Omega_C$.

The transition from LD to the LD-HD_{IN} phase in the IN region asymptotically takes the form of Eq. (23), and the one from HD to the LD-HD_{EX} phase in the EX region is obtained by particle-hole symmetry. All phase boundaries, including the IN-EX boundary (17), are thus given

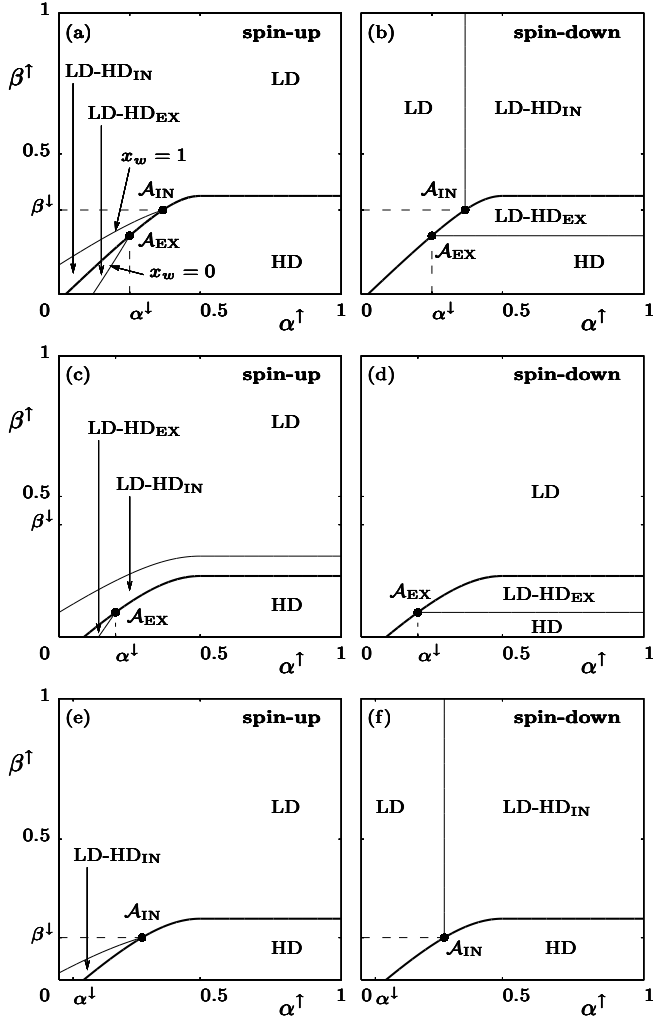


FIG. 7: Phase diagrams in the general situation: asymptotic results for large Ω . Lines of continuous transitions (thin) within the IN resp. EX region intersect the delocalization transition line (bold) in multicritical points \mathcal{A}_{IN} resp. \mathcal{A}_{EX} . Both of these points appear in (a), (b) ($\alpha^\downarrow = 0.25, \beta^\downarrow = 0.3$) while only \mathcal{A}_{EX} is present in (c), (d) ($\alpha^\downarrow = 0.2, \beta^\downarrow = 0.4$) and \mathcal{A}_{IN} alone in (e), (f) ($\alpha^\downarrow = 0.05, \beta^\downarrow = 0.15$), yielding different topologies.

by simple quadratic expressions.

Phase diagrams with different topologies that can emerge are exhibited in Fig. 7 and 8. As in the previous subsection, we show the phases of spin-up (spin-down) states on the left (right) panels. The phase boundaries between the LD and the LD-HD_{IN} phase in the IN region for spin-up as well as spin-down both intersect the IN-EX boundary in a multicritical point \mathcal{A}_{IN} , being located at $\beta^\uparrow = \beta^\downarrow$. Similarly, the lines of continuous transitions within the EX region both coincide with the IN-EX boundary in a multicritical point \mathcal{A}_{EX} , which is situated at $\alpha^\uparrow = \alpha^\downarrow$. Note that the phase transitions emerging in the density profile of spin-down within the IN region do not depend on β^\uparrow , thus being horizontal lines in the

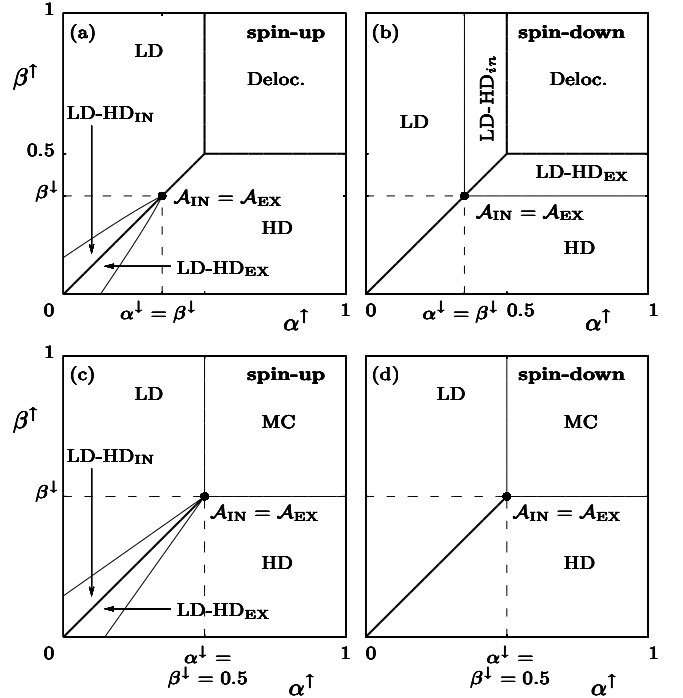


FIG. 8: Delocalization as well as maximal current phase (MC). When $\alpha^\downarrow = \beta^\downarrow < 1/2$ and $\alpha^\uparrow, \beta^\uparrow \geq 1/2$ [upper right quadrant in (a), (b)], delocalized domain walls form in the density profiles of both spin states. If instead $\alpha^\downarrow, \beta^\downarrow \geq 1/2$, the maximal current phase emerges, see (c), (d).

phase diagrams; and within the EX region they are independent of α^\uparrow , yielding vertical lines.

For $\alpha^\downarrow, \beta^\downarrow < 1/2$, Fig. 7 shows different topologies of phase diagrams, which only depend on which of the multicritical points \mathcal{A}_{IN} , \mathcal{A}_{EX} is present. If both appear, see Fig. 7 (a), (b), the LD-HD_{IN} and the LD-HD_{EX} phase for spin-up are adjacent to each other, separated by the IN-EX boundary. Although in both phases localized domain walls emerge, their position changes discontinuously upon crossing the delocalization transition. E.g., starting within the LD-HD_{IN} phase, the domain wall delocalizes when approaching the IN-EX boundary, and, having crossed it, relocates again, but at a different position.

When $\alpha^\downarrow = \beta^\downarrow < 1/2$, a subtlety emerges, see Fig. 8 (a), (b). If both $\alpha^\uparrow \geq 1/2$ and $\beta^\uparrow \geq 1/2$, i.e. in the upper right quadrant of the phase diagrams, these rates effectively act as 1/2, and Eq. (17) for the IN-EX boundary is fulfilled *in this whole region*. Therefore, delocalized domain walls form on both lanes within this region, as is confirmed by our stochastic simulations [31].

The maximal current phase (MC) emerges when all rates exceed or equal the value 1/2, corresponding to the upper left quadrant of the phase diagrams in Fig. 8 (c), (d).

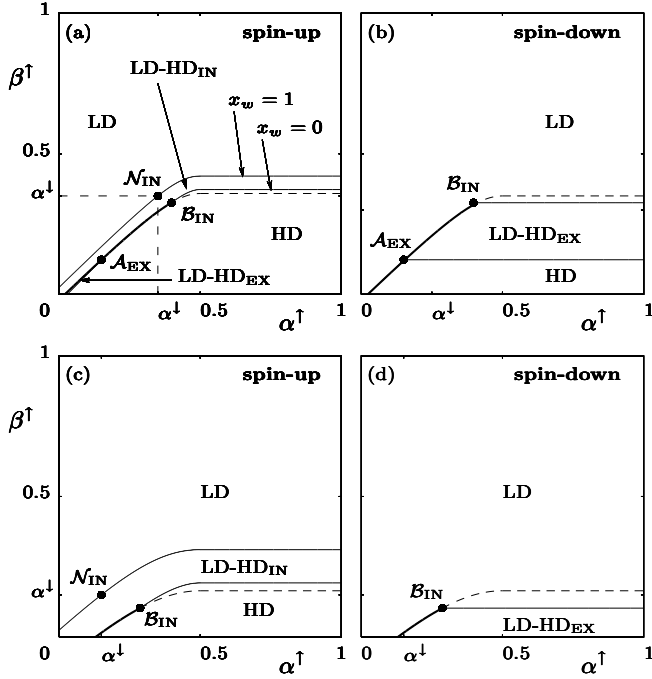


FIG. 9: Phase diagrams in the general case and small values of Ω . The nodal point \mathcal{N}_{IN} remains unchanged when Ω is varied. The appearance of the multicritical point \mathcal{B}_{IN} is accompanied by the non-occurrence of phase transitions across parts of the IN-EX boundary, then shown as dashed line. The multicritical point \mathcal{A}_{EX} emerges in (a), (b), but not in the situation of (c), (d). Parameters are $\Omega = 0.08$, $\alpha^\downarrow = 0.35$, $\beta^\downarrow = 0.45$ in (a), (b) and $\Omega = 0.2$, $\alpha^\downarrow = 0.15$, $\beta^\downarrow = 0.4$ in (c), (d).

2. Small values of Ω

When $\Omega < \Omega_C$, the transitions from LD to LD-HD_{IN} within the IN region as well as the analogue in the EX region are possible. As in the case of equal entering rates, the corresponding transition lines pairwise intersect the IN-EX boundary in multicritical points \mathcal{B}_{IN} and \mathcal{B}_{EX} . As all transitions between phases of the spin-down density within the IN region are independent of β^\uparrow , the corresponding lines are simply horizontal; and within the EX region, their independence of α^\uparrow implies that they yield vertical lines. The phase diagram for the density of spin-down is thus easily found from the IN-EX boundary given by Eq. (17) together with the locations of the multicritical points \mathcal{A}_{IN} , \mathcal{A}_{EX} , \mathcal{B}_{IN} and \mathcal{B}_{EX} . The latter follow from the intersection of phase transition lines for the density of spin-up, involving the whole analytic solution (A11), (A12), with the IN-EX boundary.

In Fig. 9 two interesting topologies that may arise are exemplified. Induced by the presence of the multicritical point \mathcal{B}_{IN} , phase transitions do not occur across all the IN-EX boundary, which is then only shown as dashed line. In Fig. 9 (a), (b), the points \mathcal{A}_{EX} and \mathcal{B}_{IN} are present. The LD-HD_{IN} phase for spin-up intervenes the LD and the HD phase; the LD-HD_{EX} phase for spin-up

is also present, though very tiny. In the phase diagram of spin-down, the LD-HD_{IN} phase intervenes the LD and the HD phase accompanied by continuous as well as discontinuous transitions. Again, the presence of the multicritical points induces the topology; e.g. in Fig. 9 (c), (d), only \mathcal{B}_{IN} appears. For the discussion of the possible topologies, we encounter the restriction that \mathcal{A}_{IN} and \mathcal{B}_{IN} cannot occur together, as well as \mathcal{A}_{EX} and \mathcal{B}_{EX} exclude each other (otherwise, the lines determined by $x_w = 0$ and $x_w = 1$ would cross).

We now discuss the influence of the spin-flip rate Ω on the continuous transition lines for spin-up. In Subsec. IV D the manifold defined by $\alpha^\uparrow = \beta^\uparrow = \alpha_{\text{eff}}^\downarrow$ was found to be a sub-manifold of the phase boundary specified by $x_w = 1$ in the IN region. Independent of Ω , the point $\alpha^\uparrow = \beta^\uparrow = \alpha_{\text{eff}}^\downarrow$, denoted by \mathcal{N}_{IN} , thus lies on the boundary between the LD and the LD-HD_{IN} phase (determined by $x_w = 1$). For large Ω , this boundary approaches the one given by Eq. (23).

Regarding the transition from the HD to the LD-HD_{IN} within the IN region (determined by $x_w = 0$), Subsec. IV D revealed that for increasing Ω it leaves the IN region at a critical transfer rate $\Omega^*(\alpha^\downarrow, \beta^\uparrow)$. In the limit $\Omega \rightarrow 0$, the densities $\rho^\uparrow(x)$ and $\rho^\downarrow(x)$ approach constant values, and both the curve $x_w = 1$ as $x_w = 0$ for spin-up in the IN region approach the line $\beta^\uparrow = \alpha^\uparrow$ for $\alpha^\uparrow \leq \frac{1}{2}$. The phase in the upper right quadrant in the phase diagram converges to the MC phase, such that in this limit, the case of two uncoupled TASEPs is recovered.

VII. CONCLUSIONS

We have presented a detailed study of an exclusion process with internal states recently introduced in [19]. The Totally Asymmetric Exclusion Process (TASEP) has been generalized by assigning two internal states to the particles. Pauli's exclusion principle allows double occupation only for particles in different internal states. Occasional switches from one internal state to the other induce a coupling between the transport processes of the separate states. Such a dynamics encompasses diverse situations, ranging from vehicular traffic on multiple lanes to molecular motors walking on intracellular tracks and future spintronics devices.

We have elaborated on the properties of the emerging non-equilibrium steady state focusing on density and current profiles. In a mesoscopic scaling of the switching rate between the internal states, nontrivial phenomena emerge. A localized domain wall in the density profile of one of the internal states induces a spontaneous polarization effect when viewing the internal states as spins. We provide an explanation based on the weakly conserved currents of the individual states and the current-density relations. A quantitative analytic description within a mean-field approximation and a continuum limit has been developed and solutions for the density and current profiles have been presented. A comparison with stochas-

tic simulations revealed that our analytic approach becomes exact in the limit of large system sizes. We have attributed this remarkable finding to the exact current-density relation in the TASEP, supplemented by the locally weak coupling of the two TASEPs appearing in our model: $\omega \rightarrow 0$ in the limit of large system sizes. Local correlations between the two internal states are thus obliterated, as particles hop forward on a much faster timescale than they switch their internal state.

Furthermore, the parameter regions that allow for the formation of a localized domain wall have been considered. Analytic phase diagrams for various scenarios, in particular the case of equal entrance rates, have been derived. The phase diagrams have been found to exhibit a rich structure, with continuous as well as discontinuous non-equilibrium phase transitions. The discontinuous one originates in the conserved particle current, which is either limited by injection or extraction of particles. At the discontinuous transition between both regimes, delocalized domain walls emerge in the density profiles of *both* internal states. Multicritical points appear at the intersections of different transition lines organizing the topology of the phase diagrams. Two classes of multicritical points are identified, one of them arises only for sufficiently small gross spin flip rate $\Omega < \Omega_C$. The value Ω_C , calculated analytically, provides a natural scale for the rate Ω .

It would be of interest to see which of the described phenomena qualitatively remain when generalizing the model to include more than two internal states. Indeed, within the context of molecular motors walking on microtubuli [7], between 12 and 14 parallel lanes are relevant. Also, the internal states might differ in the sense of different switching rates from one to another [28] and the built-in asymmetry may result in different phases. In the context of intracellular transport it appears worthwhile to investigate the consequences of a coupling to a bulk reservoir, in particular, to study the interplay of domain wall formation induced by attachment and detachment processes as well as rare switching events.

VIII. ACKNOWLEDGEMENTS

The authors gratefully acknowledge helpful discussions with Felix von Oppen, Ulrich Schollwöck, Paolo Pierobon and Mauro Mobilia.

APPENDIX A: THE DENSITIES IN THE FIRST ORDER APPROXIMATION AND THE CRITICAL VALUE Ω_C

In this Appendix, we give details on the derivation of the analytic solution of the mean-field approximation in the continuum limit to first order in ϵ , i.e. the system of differential equations (10), (11).

Summing them we find

$$\partial_x [2\rho^\uparrow(x_i) - 1]^2 + \partial_x [2\rho^\downarrow(x_i) - 1]^2 = 0, \quad (\text{A1})$$

such that

$$[2\rho^\uparrow(x_i) - 1]^2 + [2\rho^\downarrow(x_i) - 1]^2 = J, \quad (\text{A2})$$

constitutes a first integral. Remember that $j^{\text{tot}} = \rho^\uparrow(x_i)[1 - \rho^\uparrow(x_i)] + \rho^\downarrow(x_i)[1 - \rho^\downarrow(x_i)]$, such that J is given by the total current:

$$J = 2 - 4j^{\text{tot}}. \quad (\text{A3})$$

This equation suggests the following parametrization:

$$\begin{aligned} \cos \theta &= J^{-\frac{1}{2}}(2\rho^\uparrow - 1) \\ \sin \theta &= J^{-\frac{1}{2}}(2\rho^\downarrow - 1). \end{aligned} \quad (\text{A4})$$

The derivative reads

$$\frac{\sqrt{J}}{2} \cos \theta \frac{d\theta}{dx} = \frac{d\rho^\uparrow}{dx}, \quad (\text{A5})$$

which leads to the differential equation

$$\sqrt{J} \sin \theta \cos \theta \frac{d\theta}{dx} = \Omega(\sin \theta - \cos \theta). \quad (\text{A6})$$

This may be solved by a separation of variables:

$$\frac{\Omega}{\sqrt{J}} x = \int_{\theta(0)}^{\theta(x)} \frac{\sin \theta \cos \theta}{\sin \theta - \cos \theta} d\theta.$$

To perform the integral, the substitution $y = \tan \frac{\theta}{2}$ is useful. We obtain the inverse function $x = x(\theta)$:

$$x(\theta) = \frac{\sqrt{J}}{\Omega} G(y) \Big|_{y=\tan \frac{\theta}{2}} + I. \quad (\text{A7})$$

Here we defined the function $G(y)$ by

$$G(y) = \left\{ \frac{1+y}{1+y^2} + \frac{\sqrt{2}}{4} \ln \left| \frac{\sqrt{2} - (1+y)}{\sqrt{2} + 1 + y} \right| \right\}, \quad (\text{A8})$$

and I is a constant of integration.

To obtain the inverse functions $x(\rho^\uparrow)$ and $x(\rho^\downarrow)$, we have to express $\tan \frac{\theta}{2}$ by ρ^\uparrow resp. ρ^\downarrow . Recognize that $\tan \frac{\theta}{2}$ can be positive or negative. We therefore define

$$s^\downarrow = \begin{cases} -1 & \text{if } \rho^\downarrow < \frac{1}{2} \\ +1 & \text{if } \rho^\downarrow > \frac{1}{2} \end{cases}, \quad (\text{A9})$$

and analogously s^\uparrow with \uparrow and \downarrow interchanged. Now

$$\tan \frac{\theta}{2} = s^\downarrow \cdot \sqrt{\frac{1 - J^{-1/2}(2\rho^\uparrow - 1)}{1 + J^{-1/2}(2\rho^\uparrow - 1)}}. \quad (\text{A10})$$

The inverse functions $x(\rho^\uparrow)$ and $x(\rho^\downarrow)$ thus read:

$$x(\rho^\uparrow) = \frac{\sqrt{J}}{\Omega} G(y) \Big|_{y=s^\downarrow \cdot \sqrt{\frac{1-J^{-1/2}(2\rho^\uparrow-1)}{1+J^{-1/2}(2\rho^\uparrow-1)}}} + I \quad (\text{A11})$$

$$x(\rho^\downarrow) = \frac{\sqrt{J}}{\Omega} G(y) \Big|_{y=s^\uparrow \cdot \sqrt{\frac{1-J^{-1/2}(2\rho^\downarrow-1)}{1+J^{-1/2}(2\rho^\downarrow-1)}}} + I. \quad (\text{A12})$$

The constants of integration I and $J = 2 - 4j^{\text{tot}}$ are determined by matching the boundary conditions. The inverse functions of Eqs. (A11), (A12) constitute the solution to Eqs. (10) and (11), within the first-order approximation to the mean-field equations for the densities in the continuum limit.

Next, we derive the result on Ω_C given at the end of Subsec. IV D. Therefore, consider Fig. 4. We are interested in the point $x_{\frac{1}{2}}$, and thus in the right branch of the spin-up density profile. As the spin-down density is in the LD phase, i.e. it is smaller than $\frac{1}{2}$, we have $s^\downarrow = -1$ in the above solution for ρ^\uparrow . Thus, $y \leq 0$ in Eq. (A11). At the branching point of the analytic solution, i.e. the point $x_{\frac{1}{2}}$, we have the density $\frac{1}{2}$, such that there $y = -1$, implying $G(y) = 0$. Now, if this branching point lies on the right boundary, $x_{\frac{1}{2}} = 0$, as it does for the crit-

ical Ω^* , this yields $I = 0$ in Eq. (A11). On the other hand, the right branch satisfies the boundary condition on the right: $\rho^\uparrow(x=1) = 1 - \beta^\uparrow$. Upon substitution into Eq. (A11), we obtain

$$1 = x(1 - \beta^\uparrow) = \frac{\sqrt{J}}{\Omega^*} G(y) \Big|_{y=-\sqrt{\frac{1-J^{-1/2}(1-2\beta^\uparrow)}{1+J^{-1/2}(1-2\beta^\uparrow)}}}. \quad (\text{A13})$$

which for given $\alpha^\downarrow, \beta^\uparrow$ is an equation for $\Omega^*(\alpha^\downarrow, \beta^\uparrow)$. In particular, $\Omega^*(\alpha^\downarrow, \beta^\uparrow)$ is monotonically increasing in G . Investigating $G(y)$, it turns out that $G(y)$ is in turn increasing in y . Since y is bounded from above by $y = 0$, the maximal value for $G(y)$ is provided by $G(y=0) = 1 + \frac{1}{4}\sqrt{2} \ln(3 - 2\sqrt{2})$. Next, we note that $\Omega^*(\alpha^\downarrow, \beta^\uparrow)$ is an increasing function of \sqrt{J} . With the constraint that $\alpha_{\text{eff}}^\uparrow = \frac{1}{2}$, which is necessary for $x_{\frac{1}{2}} = 0$, the largest \sqrt{J} arises for $\alpha^\downarrow = 0$, i.e. $\sqrt{J} = 1$. Combining both results, the maximal value for the critical rates $\Omega^*(\alpha^\downarrow, \beta^\uparrow)$ occurs for $\alpha^\downarrow = 0$ and $y = 0$. Both conditions together yield

$$\Omega_C = 1 + \frac{1}{4}\sqrt{2} \ln(3 - 2\sqrt{2}). \quad (\text{A14})$$

Finally, we note that $\alpha^\downarrow = 0$ and $y = 0$ implies $\beta^\uparrow = 0$, such that Ω_C arises if $\alpha^\downarrow = 0$ and $\beta^\uparrow = 0$.

-
- [1] A. Barabasi and H. Stanley, *Fractal Concepts in Surface Growth* (Cambridge University Press, Cambridge, England, 1995).
 - [2] G. Deutscher, R. Zallan, and J. Adler, eds., *Percolation Structures and Processes*, vol. 5 of *Annals of the Israel Physical Society* (Adam Hilger, Bristol, 1983).
 - [3] M. Droz, Z. Rácz, and J. Schmidt, Phys. Rev. A **39**, 2141 (1989).
 - [4] D. C. Mattis and M. L. Glasser, Rev. Mod. Phys. **70**, 979 (1998).
 - [5] B. Schmittmann and R. Zia, in *Phase Transitions and Critical Phenomena*, edited by C. Domb and J. Lebowitz (Academic Press, London, 1995), vol. 17.
 - [6] C. MacDonald, J. Gibbs, and A. Pipkin, Biopolymers **6**, 1 (1968).
 - [7] J. Howard, *Mechanics of Motor Proteins and the Cytoskeleton* (Sinauer Press, Sunderland, Massachusetts, 2001).
 - [8] N. Hirokawa, Science **279**, 519 (1998).
 - [9] D. Helbing, Rev. Mod. Phys. **73**, 1067 (2001).
 - [10] D. Chowdhury, L. Santen, and A. Schadschneider, Physics Reports **329**, 199 (2000).
 - [11] B. Derrida and M. Evans, in *Nonequilibrium Statistical Mechanics in One Dimension*, edited by V. Privman (Cambridge University Press, Cambridge, 1997), pp. 277–304.
 - [12] D. Mukamel, in *Soft and Fragile Matter*, edited by M. Cates and M. Evans (Institute of Physics Publishing, Bristol, 2000), pp. 237–258.
 - [13] G. Schütz, in *Phase Transitions and Critical Phenomena*, edited by C. Domb and J. Lebowitz (Academic Press, San Diego, 2001), vol. 19, pp. 3–251.
 - [14] J. Krug, Phys. Rev. Lett. **67**, 1882 (1991).
 - [15] G. Odor, Rev. Mod. Phys. **76**, 663 (2004).
 - [16] U. C. Täuber, M. J. Howard, and H. Hinrichsen, Phys. Rev. Lett. **80**, 2165 (1998).
 - [17] J. D. Noh and H. Park, Phys. Rev. Lett. **94**, 145702 (2005).
 - [18] E. Dagotto and T. M. Rice, Science **271**, 618 (1996).
 - [19] T. Reichenbach, T. Franosch, and E. Frey, Phys. Rev. Lett. **97**, 050603 (2006).
 - [20] Žutić, J. Fabian, and S. D. Sarma, Rev. Mod. Phys. **76**, 323 (2004).
 - [21] C. K. Hahn, Y. J. Park, E. K. Kim, and S. Min, Appl. Phys. Lett. **73**, 2479 (1998).
 - [22] H. Hinsch, R. Kouyos, and E. Frey, in *Traffic and Granular Flow '05*, edited by A. Schadschneider, T. Pöschel, R. Kühne, M. Schreckenberg, and D. E. Wolf (Springer, 2006).
 - [23] V. Popkov and I. Peschel, Phys. Rev. E **64**, 026126 (2001).
 - [24] V. Popkov and G. M. Schütz, J. Stat. Phys. **112**, 523 (2003).
 - [25] V. Popkov, J. Phys. A: Math. Gen. **37**, 1545 (2004).
 - [26] E. Pronina and A. B. Kolomeisky, J. Phys. A: Math. Gen. **37**, 9907 (2004).
 - [27] T. Mitsudo and H. Hayakawa, J. Phys. A: Math. Gen. **38**, 3087 (2005).
 - [28] E. Pronina and A. B. Kolomeisky, Physica A **372**, 12 (2006).
 - [29] A. Parmeggiani, T. Franosch, and E. Frey, Phys. Rev. Lett. **90**, 086601 (2003).

- [30] A. Parmeggiani, T. Franosch, and E. Frey, Phys. Rev. E **70**, 046101 (2004).
- [31] T. Reichenbach, T. Franosch, and E. Frey, in preparation.
- [32] L. B. Shaw, R. K. P. Zia, and K. H. Lee, Phys. Rev. E **68**, 021910 (2003).
- [33] P. Pierobon, T. Franosch, and E. Frey, Phys. Rev. E **74**, 031920 (2006).
- [34] B. Derrida, Phys. Rep. **301**, 65 (1998).
- [35] The convention to flip the spin simultaneously is natural in the language of solid-state physics. In the context of two-lane traffic, it appears more natural to consider vacancies moving on the *same* lane in the reverse direction.
- [36] This situation arises in a certain neighborhood of the multicritical points \mathcal{B} , discussed in Sec. VI